UWB Ranging and IMU Data Fusion: Overview and Nonlinear Stochastic Filter for Inertial Navigation

Hashim A. Hashim, *Senior Member, IEEE*, Abdelrahman E. E. Eltoukhy, and Kyriakos G. Vamvoudakis, *Senior Member, IEEE*

***Abstract*— This paper proposes a nonlinear stochastic complementary filter design for inertial navigation that takes advantage of a fusion of Ultra-wideband (UWB) and Inertial Measurement Unit (IMU) technology ensuring semi-global uniform ultimate boundedness (SGUUB) of the closed loop error signals in mean square. The proposed filter estimates the vehicle's orientation, position, linear velocity, and noise covariance. The filter is designed to mimic the nonlinear navigation motion kinematics and is posed on a matrix Lie Group, the extended form of the Special Euclidean Group $\mathbb{SE}_2(3)$. The Lie Group based structure of the proposed filter provides unique and global representation avoiding singularity (a common shortcoming of Euler angles) as well as non-uniqueness (a common limitation of unit-quaternion). Unlike Kalman-type filters, the proposed filter successfully addresses IMU measurement noise considering unknown upper-bounded covariance. Although the navigation estimator is proposed in a continuous form, the discrete version is also presented. Moreover, the unit-quaternion implementation has been provided in the Appendix. Experimental validation performed using a publicly available real-world six-degrees-of-freedom (6 DoF) flight dataset obtained from an unmanned Micro Aerial Vehicle (MAV) illustrating the robustness of the proposed navigation technique.**

***Index Terms*— Sensor-fusion, inertial navigation, ultra-wideband ranging, inertial measurement unit, stochastic differential equation, stability, localization, observer design.**

I. Introduction

INERTIAL navigation is a fundamental robotic task commonly accomplished by fusing information from multiple sensors [1], [2], [3], [4]. Traditionally, outdoor robotic missions carried out by Unmanned Aerial Vehicles (UAVs), mobile robots, and ground vehicles utilize a combination of Global Positioning Systems (GPS) and an Inertial Measurement Unit (IMU) to extract the navigation components, namely vehicle's orientation (commonly known as attitude), position, and linear velocity, essential for the success of any control missions [5]. However, GPS signal is susceptible to obstructions, multipath, fading, and/or denial (indoor mission and in harsh weather). Given the possibility of GPS signal loss, availability of a back-up technology for accurate estimation of the navigation components is crucial to prevent mission failure until GPS signal is restored. As such, the research community has been actively seeking to address the above challenge using different Inertial Navigation Systems (INSs). For instance, vision-based aided navigation techniques that rely on a vision unit (monocular or stereo camera) and an IMU have been employed [1], [2], [6], [7]. Other researchers have integrated a Light Detection and Ranging (LiDAR) sensor and an IMU [3]. Navigation components estimation can also be enabled by fusing an Ultra-wideband (UWB) and an IMU [4], [8], [9]. In comparison with LiDAR and vision units, UWB and IMU fusion reduces the cost, size, and weight of the sensing unit and the power requirements. Moreover, UWB enables positioning whether the communication between the tag (attached to the robot) and the fixed anchors (source) is within the Line-of-sight (LOS) or Non-line-of-sight (NLOS). However, the main challenge of using a combination of UWB and IMU is their proneness to measurement uncertainties [10], [11], [12], [13].

Localization of a rigid-body (e.g., UAVs and ground vehicles) aims to fully define attitude and position [2]. A vehicle equipped with a 9-axis IMU (composed of a gyroscope, an accelerometer, and a magnetometer) allows for attitude determination. A vehicle equipped with a tag accessed by a group of fixed anchors allows for position determination. Attitude and position determination are normally impaired by noise, and therefore, require a robust filter to (1) attenuate the noise effect, (2) estimate the hidden states (the linear velocity), and (3) produce reasonable navigation estimates. Over the last few years, several Gaussian navigation filters have been proposed based on the fusion of UWB and IMU to achieve higher estimation accuracy and reduce measurement noise. Examples of IMU-UWB-based Gaussian navigation filters include a Kalman Filter (KF) that has been developed for indoor localization systems [14], a tightly coupled Extended Kalman Filter (EKF) that addresses the divergence of KFs [15], [16], and an Unscented Kalman Filter (UKF) suited for a group of unmanned ground vehicles that uses a set of sigma points to improve the probability distribution [4].

Manuscript received 16 August 2022; revised 21 April 2023, 19 June 2023, and 17 August 2023; accepted 23 August 2023. This work was supported in part by the National Sciences and Engineering Research Council of Canada (NSERC) under Grant RGPIN-2022-04937; and in part by the National Science Foundation under Grant S&AS-1849264, Grant CPS-1851588, and Grant CPS-2038589. The Associate Editor for this article was H. Jiang. *(Corresponding author: Hashim A. Hashim.)*

Hashim A. Hashim is with the Department of Mechanical and Aerospace Engineering, Carleton University, Ottawa, ON K1S 5B6, Canada (e-mail: hhashim@carleton.ca).

Abdelrahman E. E. Eltoukhy is with the Department of Management Science and Engineering, Khalifa University, Abu Dhabi, United Arab Emirates (e-mail: abdelrahman.eltoukhy@polyu.edu.hk).

Kyriakos G. Vamvoudakis is with the Daniel Guggenheim School of Aerospace Engineering, Georgia Institute of Technology, Atlanta, GA 30332 USA (e-mail: kyriakos@gatech.edu).

Digital Object Identifier 10.1109/TITS.2023.3309288

In addition, Particle filters (PFs) reliant on IMU-UWB-fusion have been introduced [8]. PFs do not follow the Gaussian assumption and they are typically classified as stochastic filters [17]. The main shortcoming of KF, EKF, and UKF, is the fact that they are based on optimal minimum-energy which is first order adopting linearization around a nominal point [17], [18]. As such, higher order terms are disregarded resulting in degradation of the estimation accuracy. Furthermore, UKF sigma points add complexity to the implementation process [17]. The limitations of PFs are two-fold: 1) they have higher computational cost (unfit for small scale systems) [17], and 2) the stability results are not indicative of the proximity of the solution to the optimal one [18], [19]. In addition, the KF, EKF, UKF and PF techniques utilize Euler angles which are subject to singularities. It is critical to consider that the navigation kinematics of a vehicle moving in three-dimensional (3D) space are highly nonlinear. As such, to capture the nonlinearity and address the singularity issue of Euler angles, the navigation problem is best modeled on the Lie Group. Moreover, the impracticality of the known noise covariance assumption adopted by Kalman-type filters and PFs has to be addressed [17], [20].

Motivated by the advantages and limitations of the above literature discussion, this work aims to capture the complex nonlinear nature of the navigation kinematics. Hence, the problem is modeled on the Lie Group of the extended form of the Special Euclidean Group $\mathbb{SE}_2(3)$. The navigation approach proposed in this work makes provision for the uncertainty in IMU measurements and considers a vehicle equipped with a UWB tag and availability of n UWB anchors. Consequently, the contributions of this work are as follows:

1) A nonlinear stochastic complementary filter for inertial navigation developed on the Lie Group of $\mathbb{SE}_2(3)$ reliant on the direct UWB and IMU measurements is proposed.
2) The filter is characterized with a geometric framework, able to preserve the Lie Group and avoid singularity unlike Gaussian navigation filters.
3) The stochastic filter effectively addresses unknown measurement noise introduced by an IMU.
4) The proposed filter guarantees semi-global uniform ultimate boundedness (SGUUB) of the closed loop error signals in mean square using Lyapunov stability.

The paper is composed of seven Sections and an Appendix. Section II presents preliminaries and the related math notation. Section III details the UWB positioning problem, orientation determination using IMU, and the navigation estimation problem. Section IV presents the proposed nonlinear stochastic navigation filter design on $\mathbb{SE}_2(3)$. Section V illustrates the possibility of position and orientation determination using solely UWB technology conditioned on potential advancement of UWB ranging accuracy. Section VI demonstrates the robustness of the proposed approach by means of testing it on a real-world dataset. Finally, Section VII concludes the work.

II. Preliminaries

Throughout this paper $\mathbb{R}_+$ refers to the set of nonnegative real numbers. For $v \in \mathbb{R}^n$ and $Q \in \mathbb{R}^{n\times m}$, the Euclidean

TABLE I

Nomenclature

$\mathbb{R}^{n\times m}$	:	n-by-m real dimensional space
$\mathbb{SO}(3)$	:	Special Orthogonal Group
$\mathfrak{so}(3)$	:	Lie-algebra of $\mathbb{SO}(3)$
$\mathbb{SE}_2(3)$	:	Extended Special Euclidean Group, $\mathbb{SE}_2(3) = \mathbb{SO}(3) \times \mathbb{R}^3 \times \mathbb{R}^3$
$\mathbb{S}^3$	:	Three-unit-sphere
h_i	:	ith UWB Anchor (source) position, $h_i \in \mathbb{R}^3$
P	:	Unknown vehicle (UWB Tag) position, $P \in \mathbb{R}^3$
$\hat{P}$	:	Estimated vehicle position, $\hat{P} \in \mathbb{R}^3$
R and $\hat{R}$	:	True (unknown) and estimated attitude, $R, \hat{R} \in \mathbb{SO}(3)$
V and $\hat{V}$	:	True (unknown) and estimated linear velocity, $V, \hat{V} \in \mathbb{R}^3$
Ω and Ω_m	:	True and measured angular velocity, $\Omega, \Omega_m \in \mathbb{R}^3$
a and a_m	:	True and measured acceleration, $a, a_m \in \mathbb{R}^3$
X and $\hat{X}$	:	True (unknown) and estimated navigation, $X, \hat{X} \in \mathbb{SE}_2(3)$
P_y	:	Reconstructed position, $R_y \in \mathbb{R}^3$
$\tilde{R}$	:	Attitude estimation error, $\tilde{R} \in \mathbb{SO}(3)$
$\tilde{P}$ and $\tilde{V}$	:	Position and linear velocity estimation error, $\tilde{P}, \tilde{V} \in \mathbb{R}^3$

norm of v is described by $||v|| = \sqrt{v^\top v}$ and the Frobenius norm of Q is defined by $||Q||_F = \sqrt{\text{Tr}\{QQ^*\}}$ where $*$ is a conjugate transpose. $\mathbf{I}_n$ represents an n-by-n identity matrix and $0_{n\times m}$ describes an n-by-m zero matrix. For $M_r \in \mathbb{R}^{n\times n}$, $\lambda(M_r) = \{\lambda_1, \lambda_2, \ldots, \lambda_n\}$ describes the set of eigenvalues of M_r with $\overline{\lambda}_{M_r} = \overline{\lambda}(M_r)$ referring to the maximum eigenvalue and $\underline{\lambda}_{M_r} = \underline{\lambda}(M_r)$ being the minimum eigenvalue of M_r. $\det(\cdot)$ denotes a determinant, $\exp(\cdot)$ represents exponential, and $\mathbb{E}[\cdot]$ refers to an expected value. $\{\mathcal{I}\}$ describes fixed inertial-frame and $\{\mathcal{B}\}$ represents body-frame fixed to the navigating vehicle. The Special Orthogonal Group $\mathbb{SO}(3)$ is described by [17] and [21]

$$\mathbb{SO}(3) = \left\{ R \in \mathbb{R}^{3\times 3} \middle| R^\top R = RR^\top = \mathbf{I}_3, \det(R) = +1 \right\}$$

where $R \in \mathbb{SO}(3)$ refers to vehicle's orientation (attitude) in the $\{\mathcal{B}\}$-frame. The Lie algebra of $\mathbb{SO}(3)$ is denoted as $\mathfrak{so}(3)$ such that

$$\mathfrak{so}(3) = \{[v]_\times \in \mathbb{R}^{3\times 3} | [v]_\times^\top = -[v]_\times, v \in \mathbb{R}^3\}$$
$$[v]_\times = \begin{bmatrix} 0 & -v_3 & v_2 \\ v_3 & 0 & -v_1 \\ -v_2 & v_1 & 0 \end{bmatrix} \in \mathfrak{so}(3), \quad v = \begin{bmatrix} v_1 \\ v_2 \\ v_3 \end{bmatrix}$$

where $[v]_\times$ describes a skew symmetric matrix. $\mathbf{vex} : \mathfrak{so}(3) \to \mathbb{R}^3$ represents the inverse mapping of $[\cdot]_\times$ such that $\mathbf{vex}([v]_\times) = v, \forall v \in \mathbb{R}^3$. The anti-symmetric projection on $\mathfrak{so}(3)$ is described by $\boldsymbol{\mathcal{P}}_a(M_r) = \frac{1}{2}(M_r - M_r^\top) \in \mathfrak{so}(3), \forall M_r \in \mathbb{R}^{3\times 3}$. For $M_r \in \mathbb{R}^{3\times 3}$, $\boldsymbol{\Upsilon} = \mathbf{vex} \circ \boldsymbol{\mathcal{P}}_a$ represents a composition mapping with $\boldsymbol{\Upsilon}(M_r) = \mathbf{vex}(\boldsymbol{\mathcal{P}}_a(M_r)) \in \mathbb{R}^3$. The Euclidean distance of thr vehicle's orientation $R \in \mathbb{SO}(3)$ is defined by

$$||R||_{\text{I}} = \text{Tr}\{\mathbf{I}_3 - R\}/4 \in [0, 1] \tag{1}$$

with $-1 \leq \mathrm{Tr}\{R\} \leq 3$ and $||R||_{\mathrm{I}} = \frac{1}{8}||\mathbf{I}_3 - R||_F^2$, refer to [17]. Likewise, we define $||MR||_{\mathrm{I}} = \mathrm{Tr}\{M - MR\}/4$ for all $M \in \mathbb{R}^{3\times 3}$. Consider a vehicle navigating in 3D space where $R \in \mathbb{SO}(3)$, $P \in \mathbb{R}^3$, and $V \in \mathbb{R}^3$ denote its attitude, position, and velocity, respectively, with $R \in \{\mathcal{B}\}$ and $P, V \in \{\mathcal{I}\}$. Define $\mathbb{SE}_2(3) = \mathbb{SO}(3) \times \mathbb{R}^3 \times \mathbb{R}^3 \subset \mathbb{R}^{5\times 5}$ [22] add later as the extended form of the Special Euclidean Group $\mathbb{SE}(3) = \mathbb{SO}(3) \times \mathbb{R}^3 \subset \mathbb{R}^{4\times 4}$ with

$$\mathbb{SE}_2(3) = \{X \in \mathbb{R}^{5\times 5} \big| R \in \mathbb{SO}(3), P, V \in \mathbb{R}^3\} \quad (2)$$

$$X = \Psi(R, P, V) = \begin{bmatrix} R & P & V \\ 0_{1\times 3} & 1 & 0 \\ 0_{1\times 3} & 0 & 1 \end{bmatrix} \in \mathbb{SE}_2(3) \quad (3)$$

$X \in \mathbb{SE}_2(3)$ is known as a homogeneous navigation matrix. $T_X\mathbb{SE}_2(3) \in \mathbb{R}^{5\times 5}$ is the tangent space of $\mathbb{SE}_2(3)$ at point X. Let us introduce a submanifold $\mathcal{U}_{\mathcal{M}} = \mathfrak{so}(3) \times \mathbb{R}^3 \times \mathbb{R}^3 \times \mathbb{R} \subset \mathbb{R}^{5\times 5}$ where

$$\mathcal{U}_{\mathcal{M}} = \left\{u([\Omega]_\times, V, a, \varepsilon) | \, [\Omega]_\times \in \mathfrak{so}(3), V, a \in \mathbb{R}^3, \varepsilon \in \mathbb{R}\right\}$$

$$u([\Omega]_\times, V, a, \varepsilon) = \begin{bmatrix} [\Omega]_\times & V & a \\ 0_{1\times 3} & 0 & 0 \\ 0_{1\times 3} & \varepsilon & 0 \end{bmatrix} \in \mathcal{U}_{\mathcal{M}} \subset \mathbb{R}^{5\times 5} \quad (4)$$

such that $\Omega \in \mathbb{R}^3$, $V \in \mathbb{R}^3$, and $a \in \mathbb{R}^3$ refer to vehicle's true angular velocity, linear velocity, and apparent acceleration respectively. Note that $\Omega, a \in \{\mathcal{B}\}$. For more details on $\mathbb{SE}_2(3)$ and $\mathcal{U}_{\mathcal{M}}$ visit [2]. Let $y \in \mathbb{R}^3$, $M \in \mathbb{R}^{3\times 3}$, and $R \in \mathbb{SO}(3)$. The following identities hold:

$$[Ry]_\times = R[y]_\times R^\top \quad (5)$$

$$\mathrm{Tr}\{M[y]_\times\} = \mathrm{Tr}\{\mathcal{P}_a(M)[y]_\times\} = -2\mathbf{vex}(\mathcal{P}_a(M))^\top y \quad (6)$$

III. Problem Formulation

UWB technology has several notable advantages making it an excellent candidate for a variety of applications. The UWB signal has large bandwidth with short life-time (frequency is inversely proportional with time) which results in reasonable positioning accuracy [10]. The distinguishing feature of the UWB signal is its short wavelength allowing it to be robust against multipath interference and fading unlike GPS signal. has UWB low power consumption and fast communication speed. Additionally, the UWB signals can penetrate obstacles providing localization in LOS and NLOS. New technologies shows UWB precision of approximately 10 centimeters within ranging distance of 100 meters. Finally, UWB technology hardware is compact and allows for low-cost implementation [10], [11], [12]. However, similarly to IMU, a significant limitation of UWB is a high level of measurement noise. To gain understanding of UWB technology, let us define terms "anchor" and "tag". An anchor refers to a fixed UWB sensor with a known location, while a tag stands for a UWB attached to a navigating vehicle. A tag generally has to exchange signals with multiple anchors to determine its position in 3D space.

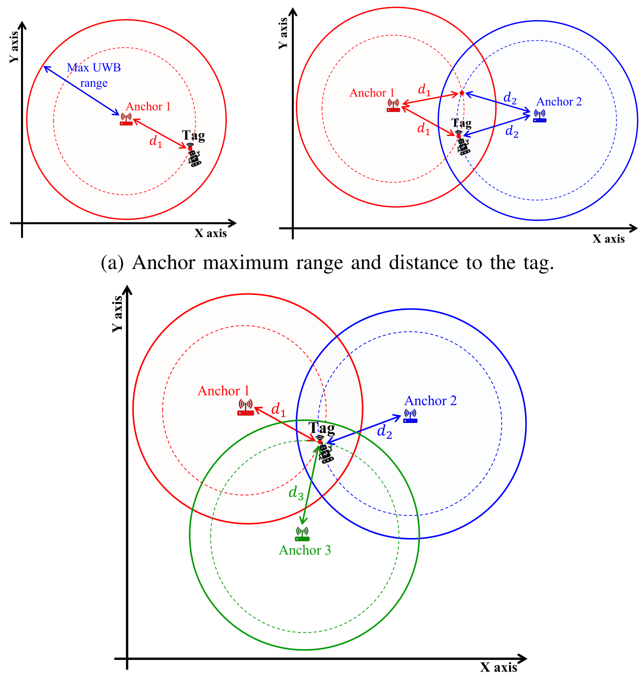

(a) Anchor maximum range and distance to the tag.

(b) Positioning in 2D space.

Fig. 1. Positioning with UWB.

A. UWB and Time of Arrival

Time of Arrival (TOA) is a well known approach that uses instant time between transmitter and receiver (travel time) to provide range or distance between anchor and tag, as long as the tag is in the range of the transmitted signal [23]. Let d_i denote the ith distance between the tag and the ith anchor. The left portion of Fig. 1.(a) illustrates maximum range of an anchor and the distance between an anchor and the tag.

Unique position determination of the tag in 2D space requires a minimum of 3 anchors. As illustrated by the left portion of Fig. 1.(a), knowledge of the range of one anchor allows to identify a circle where the tag could be potentially located. Two anchors narrow the potential location of the tag down to two options (left portion of Fig. 1.(a)). Finally, introducing the third anchor allows to precisely pinpoint the position of the tag in 2D space as illustrated in Fig. 1.(b). By extension, a minimum of 4 anchors is required to uniquely position the tag in 3D space.

Let us define the range d_i in 3D space between the fixed ith anchor positioned at $h_i = [x_i, y_i, z_i]^\top \in \mathbb{R}^3$ and the moving vehicle (UWB tag position) located at $P = [x, y, z]^\top \in \mathbb{R}^3$ as follows:

$$\begin{aligned} d_i &= ||h_i - P|| \\ &= \sqrt{(x_i - x_p)^2 + (y_i - y_p)^2 + (z_i - z_p)^2} \end{aligned} \quad (7)$$

The expression in (7) can be squared as follows:

$$d_i^2 = ||h_i||^2 + ||P||^2 - 2h_i^\top P \quad (8)$$

As such, for $j \neq i$, in view of (7) and (8), one has

$$d_j^2 = ||h_j||^2 + ||P||^2 - 2h_j^\top P \quad (9)$$

Hence, from (8) and (9) where $i = 1$ and $j = 2$, one shows $d_1^2 - d_2^2 + ||h_2||^2 - ||h_1||^2 = 2(h_2 - h_1)^\top P$. Hence, one shows

$$\underbrace{\begin{bmatrix} h_2^\top - h_1^\top \\ h_3^\top - h_1^\top \\ \vdots \\ h_N^\top - h_1^\top \end{bmatrix}}_{A} P = \frac{1}{2} \underbrace{\begin{bmatrix} d_1^2 - d_2^2 + ||h_2||^2 - ||h_1||^2 \\ d_1^2 - d_3^2 + ||h_3||^2 - ||h_1||^2 \\ \vdots \\ d_1^2 - d_N^2 + ||h_N||^2 - ||h_1||^2 \end{bmatrix}}_{B}$$

where N denotes the number of fixed anchors accessed by the tag. Defining $\delta = \frac{1}{2}(AP - B)^\top(AP - B)$ and applying the Minimum Mean Square Error (MMSE) method, one obtains $\frac{\partial \delta}{\partial P} = A^\top(AP - B) = 0$ such that

$$P = (A^\top A)^{-1} A^\top B \tag{10}$$

Assumption 1: To guarantee that the vehicle position P is uniquely defined and $(A^\top A)^{-1}$ is nonsingular, the tag must be within range of at least 4 anchors ($N \geq 4$) for positioning in 3D space and at least 3 anchors ($N \geq 3$) for positioning in 2D space.

B. UWB and Time Difference Of Arrival

TOA-based range measurements rely on synchronization between the tag and the anchor nodes. As such, the implementation of a TOA system is rather complex and is rarely used in practice. Time Difference Of Arrival (TDOA) approach, on the other hand, circumvents the need for synchronization and thereby is a common choice [24], [25]. TDOA defines the ranging distance as the difference between arrival time of a transmitted signal from two source anchors to the target tag. Based on the TDOA approach, the range distance $d_{j,i}$ between the UWB tag positioned at $P = [x, y, z]^\top \in \mathbb{R}^3$ (attached to the vehicle) and the two anchors positioned at $h_i = [x_i, y_i, z_i]^\top \in \mathbb{R}^3$ and $h_j = [x_j, y_j, z_j]^\top \in \mathbb{R}^3$ is defined as follows:

$$d_{j,i} = ||P - h_j|| - ||P - h_i|| \tag{11}$$

The expression in (11) can be squared such that

$$\frac{d_{j,i}^2 + ||h_i||^2 - ||h_j||^2}{2} = (h_i - h_j)^\top P - d_{j,i}||P - h_i|| \tag{12}$$

One way to localize the tag involves using the range difference between the main Base Station (BS) and other BSs. Fig. 2.(a) illustrates the topology of TDOA-based localization system composed of a main BS (anchor 1), other BSs (anchor 2, 3, 4), and the tag. From (11) and (12), considering N TDOA measurements, one has

$$\underbrace{\begin{bmatrix} (h_1 - h_2)^\top & -d_{2,1} \\ (h_1 - h_3)^\top & -d_{3,1} \\ \vdots & \vdots \\ (h_1 - h_N)^\top & -d_{N,1} \end{bmatrix}}_{A} \overline{P} = \frac{1}{2} \underbrace{\begin{bmatrix} d_{2,1}^2 + ||h_1||^2 - ||h_2||^2 \\ d_{3,1}^2 + ||h_1||^2 - ||h_3||^2 \\ \vdots \\ d_{N,1}^2 + ||h_1||^2 - ||h_N||^2 \end{bmatrix}}_{B}$$

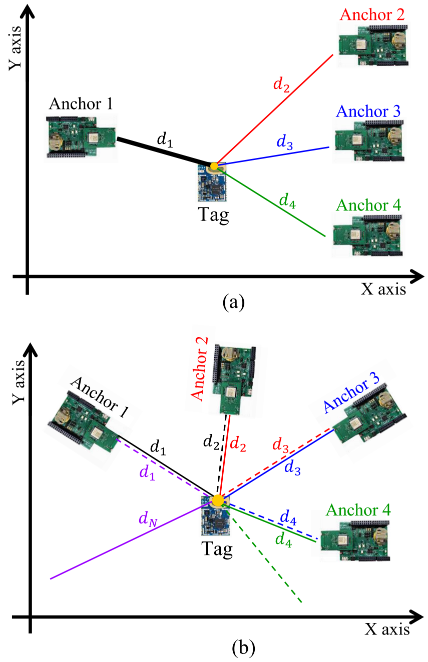

Fig. 2. Topology of TDOA-based localization system.

where N represents the number of fixed anchors accessed by the tag and $\overline{P} = [P^\top, ||P - h_1||]^\top \in \mathbb{R}^4$. Defining $\delta = \frac{1}{2}(AP - B)^\top(AP - B)$ and applying MMSE, one can show that $\frac{\partial \delta}{\partial P} = A^\top(AP - B) = 0$ with

$$\overline{P} = (A^\top A)^{-1} A^\top B \tag{13}$$

Alternatively, positioning can be achieved without utilizing a main BS station as presented in Fig. 2.(b). From the expressions in (11) and (12), and for N TDOA measurements, one obtains

$$\begin{aligned} \frac{d_{2,1}^2 + ||h_1||^2 - ||h_2||^2}{2} &= (h_1 - h_2)^\top P - d_{2,1}||P - h_1|| \\ \frac{d_{3,2}^2 + ||h_2||^2 - ||h_3||^2}{2} &= (h_2 - h_3)^\top P - d_{3,2}||P - h_2|| \\ &\vdots \\ \frac{d_{1,N}^2 + ||h_N||^2 - ||h_1||^2}{2} &= (h_N - h_1)^\top P - d_{1,N}||P - h_N|| \end{aligned} \tag{14}$$

Since, $||P - h_3|| = d_{3,2} + ||P - h_2||$, one shows

$$||P - h_3|| = d_{3,2} + d_{2,1} + ||P - h_1||$$

Likewise, one finds

$$||P - h_4|| = d_{4,3} + d_{3,2} + d_{2,1} + ||P - h_1||$$

Therefore, for N TDOA measurements

$$||P - h_N|| = \sum_{i=2}^{N} d_{i,i-1} + ||P - h_1||$$

Let us define:

$$A = \begin{bmatrix} (h_1 - h_2)^\top & -d_{2,1} \\ (h_2 - h_3)^\top & -d_{3,2} \\ \vdots & \vdots \\ (h_{N-1} - h_N)^\top & -d_{N,N-1} \\ (h_N - h_1)^\top & -d_{1,N} \end{bmatrix}$$

$$B = \frac{1}{2}\begin{bmatrix} d_{2,1}^2 + ||h_1||^2 - ||h_2||^2 \\ d_{3,2}^2 + ||h_2||^2 - ||h_3||^2 + 2d_{3,2}\sum_{i=2}^{2} d_{i,i-1} \\ d_{4,3}^2 + ||h_3||^2 - ||h_4||^2 + 2d_{4,3}\sum_{i=2}^{3} d_{i,i-1} \\ \vdots \\ d_{1,N}^2 + ||h_N||^2 - ||h_1||^2 + 2d_{1,N}\sum_{i=2}^{N} d_{i,i-1} \end{bmatrix}$$

with N being the number of fixed anchors accessed by the tag and $\overline{P} = [P^\top, ||P - h_1||]^\top \in \mathbb{R}^4$. Hence, the position determination is as follows:

$$\overline{P} = (A^\top A)^{-1} A^\top B \tag{15}$$

Note that Assumption 1 holds for the TDOA approach.

C. Inertial Measurement Unit

A typical IMU is composed of three sensors: a gyroscope, an accelerometer, and a magnetometer which are sufficient for attitude determination [5], [17], [26]. The gyroscope provides vehicle's angular velocity measurements in the $\{\mathcal{B}\}$-frame:

$$\Omega_m = \Omega + n_\Omega \in \mathbb{R}^3 \tag{16}$$

where Ω represents the true angular velocity and n_Ω stands for unknown noise in measurements, for all $\Omega_m, n_\Omega \in \{\mathcal{B}\}$. The accelerometer provides measurements of the apparent acceleration:

$$a_m = R^\top(\dot{V} - \overrightarrow{\mathrm{g}}) + n_a \in \mathbb{R}^3 \tag{17}$$

where $\overrightarrow{\mathrm{g}} = [0, 0, g]^\top$ and $\dot{V}$ denote the gravitational acceleration and the linear acceleration, respectively, with respect to $\{\mathcal{I}\}$-frame. n_a describes unknown measurement noise. Note that $\overrightarrow{\mathrm{g}}$ is described in the North-East-Down (NED) frame $\forall a_m, n_a \in \{\mathcal{B}\}$. At a low frequency, $|\overrightarrow{\mathrm{g}}| \gg |\dot{V}|$ and the accelerometer measurements can be described as $a_m \approx -R^\top \overrightarrow{\mathrm{g}} + n_a$. The magnetometer measurements can be represented by

$$m_m = R^\top m_r + n_m \in \mathbb{R}^3 \tag{18}$$

where $m_r = [m_N, 0, m_D]^\top \in \{\mathcal{I}\}$ denotes the earth-magnetic field in the NED frame and n_m represents the additive unknown noise components, $\forall m_m, \omega_m \in \{\mathcal{B}\}$. For the sake of attitude orthogonality, normalization of IMU vector measurements (a_m, m_m) and observations $(\dot{V} - \overrightarrow{\mathrm{g}}, m_r)$ is commonly employed as follows:

$$\begin{cases} \upsilon_1 = \dfrac{a_m}{||a_m||}, & r_1 = \dfrac{-\overrightarrow{\mathrm{g}}}{||-\overrightarrow{\mathrm{g}}||} \\ \upsilon_2 = \dfrac{m_m}{||m_m||}, & r_2 = \dfrac{m_r}{||m_r||} \\ \upsilon_3 = \dfrac{\upsilon_1 \times \upsilon_2}{||\upsilon_1 \times \upsilon_2||}, & r_3 = \dfrac{r_1 \times r_2}{||r_1 \times r_2||} \end{cases} \tag{19}$$

The expression in (19) ensures availability of 3 non-collinear measurements/observations necessary for attitude estimation [5], [17], [26].

D. Navigation Problem

The true navigation kinematics of a vehicle traveling in 3D space are defined by

$$\begin{cases} \dot{R} = R\,[\Omega]_\times \\ \dot{P} = V \\ \dot{V} = Ra + \overrightarrow{\mathrm{g}}, \end{cases} \qquad \underbrace{\dot{X} = XU - \mathcal{G}X}_{\text{Compact form}} \tag{20}$$

with $R \in \mathbb{SO}(3)$ being the true attitude, $P \in \mathbb{R}^3$ being the true position, $V \in \mathbb{R}^3$ being the true linear velocity, $\Omega \in \mathbb{R}^3$ being the true angular velocity, $\overrightarrow{\mathrm{g}}$ denoting the gravity vector, and $a \in \mathbb{R}^3$ being the apparent acceleration (all non-gravitational forces on the vehicle) for all $R, \Omega, a \in \{\mathcal{B}\}$ and $P, V \in \{\mathcal{I}\}$. The right portion of (20) represents the navigation kinematics in a compact form with $X \in \mathbb{SE}_2(3)$ as per the map defined in (4), while $U = u([\Omega]_\times, 0_{3\times1}, a, 1) \in \mathcal{U}_m$, and $\mathcal{G} = u(0_{3\times3}, 0_{3\times1}, -\overrightarrow{\mathrm{g}}, 1) \in \mathcal{U}_m$ as per the map defined in (4). For more information see [2]. In view of the navigation model in (20), the measurements of Ω and a are given by

$$\begin{cases} \Omega_m = \Omega + n_\Omega \in \mathbb{R}^3 \\ a_m = a + n_a \in \mathbb{R}^3 \end{cases} \tag{21}$$

where n_Ω and n_a refer to Gaussian unknown bounded and zero-mean noise. Since, derivative of a Gaussian process lead to a Gaussian process [27], [28], the noise can be redefined as $n_\Omega = \mathcal{Q}d\beta_\Omega/dt$ and $n_a = \mathcal{Q}d\beta_a/dt$, function of Brownian motion process vectors [17], [29] where $\mathcal{Q} = \mathrm{diag}(\mathcal{Q}_{1,1}, \mathcal{Q}_{2,2}, \mathcal{Q}_{3,3}) \in \mathbb{R}^{3\times3}$ refers to an unknown diagonal matrix (diagonal is positive and time-variant) and $\mathrm{diag}(\cdot)$ refers to a diagonal of a matrix. Thus, the covariance of n_Ω and n_a is given by $\mathcal{Q}^2 = \mathcal{Q}\mathcal{Q}^\top$ (for more details visit [17]). In view of (1), (20), and (21), the kinematics in (20) can be re-expressed to follow stochastic differential equations as follows:

$$\begin{cases} d||R||_{\mathrm{I}} = (1/2)\mathbf{vex}(\boldsymbol{\mathcal{P}}_a(R))^\top(\Omega_m dt - \mathcal{Q}d\beta_\Omega) \\ dP = V dt \\ dV = (Ra_m + \overrightarrow{\mathrm{g}})dt - R\mathcal{Q}d\beta_a \end{cases} \tag{22}$$

with $\mathrm{Tr}\{R[\Omega_m]_\times\} = -2\mathbf{vex}(\boldsymbol{\mathcal{P}}_a(R))^\top\Omega_m$ as defined in (6). This means that (22) is described by

$$dx = f dt + h\overline{\mathcal{Q}}d\beta \tag{23}$$

with $x = [||R||_{\mathrm{I}}, P^\top, V^\top]^\top \in \mathbb{R}^7$, $f = [(1/2)\mathbf{vex}(\boldsymbol{\mathcal{P}}_a(R))^\top\Omega_m, V^\top, (Ra_m + \overrightarrow{\mathrm{g}})^\top]^\top \in \mathbb{R}^7$, and $h\overline{\mathcal{Q}}d\beta = [(1/2)\mathbf{vex}(\boldsymbol{\mathcal{P}}_a(R))^\top d\beta_\Omega^\top\mathcal{Q}, 0_{3\times1}^\top, d\beta_a^\top\mathcal{Q}]^\top \in \mathbb{R}^7$. Let us define the following variable:

$$\sigma = [\sup_{t\geq0}\mathcal{Q}_{1,1}, \sup_{t\geq0}\mathcal{Q}_{2,2}, \sup_{t\geq0}\mathcal{Q}_{3,3}]^\top \in \mathbb{R}^3 \tag{24}$$

Definition 1 [17], [30]: Recall the stochastic kinematics in (23). The state vector $x(t)$ is almost SGUUB if for initial state $x(t_0)$ and a known set $\Xi \in \mathbb{R}^7$ there is a positive constant k_c and a time constant $t_c = t_c(x(t_0))$ with $\mathbb{E}[||x(t_0)||] < k_c, \forall t > t_0 + k_c$.

Lemma 1 [31]: Recall the stochastic differential system in (23) and consider $\mathbb{U}(x)$ to be a twice differentiable cost function where $\mathbb{U} : \mathbb{R}^7 \to \mathbb{R}_+$ such that

$$\mathcal{L}\mathbb{U}(x) = (\frac{\partial\mathbb{U}}{\partial x})^\top f + \frac{1}{2}\mathrm{Tr}\{h\overline{\mathcal{Q}}^2 h^\top \frac{\partial^2\mathbb{U}}{\partial x^2}\} \tag{25}$$

with $\mathcal{L}\mathbb{U}$ referring to a differential operator. Let us define $\alpha_1(\cdot)$ and $\alpha_2(\cdot)$ as class $\mathcal{K}_\infty$ functions and define the following constants $z_1 > 0$ and $z_2 \geq 0$ such that

$$\alpha_1(x) \leq \mathbb{U}(x) \leq \alpha_2(x) \tag{26}$$

$$\mathcal{L}\mathbb{U}(x) \leq -z_1\mathbb{U}(x) + z_2 \tag{27}$$

Therefore, the stochastic kinematics in (22) have an almost unique strong solution on $[0,\infty)$ and the solution x is bounded in probability where

$$\mathbb{E}[\mathbb{U}(x)] \leq \mathbb{U}(x(0))\exp(-z_1 t) + z_2/z_1 \tag{28}$$

ensuring that x is SGUUB in the mean square.

Lemma 2 [21]: Consider $R \in \mathbb{SO}(3)$ and $M_r = M_r^\top \in \mathbb{R}^{3\times 3}$ and define $\overline{M_r} = \mathrm{Tr}\{M_r\}\mathbf{I}_3 - M_r$ with $\overline{\lambda}_{\overline{M_r}}$ and $\underline{\lambda}_{\overline{M_r}}$ referring to the minimum and maximum eigenvalues of $\overline{M_r}$, respectively. Let $||M_r R||_{\mathrm{I}} = \frac{1}{4}\mathrm{Tr}\{M_r(\mathbf{I}_3 - R)\}$ and $\boldsymbol{\Upsilon}(M_r R) = \mathbf{vex}(\boldsymbol{\mathcal{P}}_a(M_r R))$. Thus, one obtains

$$||\boldsymbol{\Upsilon}(M_r R)||^2 \leq 2\overline{\lambda}_{\overline{M_r}}||M_r R||_{\mathrm{I}} \tag{29}$$

$$||\boldsymbol{\Upsilon}(M_r R)||^2 \geq \frac{\underline{\lambda}_{\overline{M_r}}}{2}||M_r R||_{\mathrm{I}}(1 + \mathrm{Tr}\{R\}) \tag{30}$$

IV. Stochastic Navigation Filter

In this section, a novel nonlinear stochastic complementary filter that operates based on the fusion of UWB and IMU measurements is proposed. Let $\hat{R} \in \mathbb{SO}(3)$, $\hat{P} \in \mathbb{R}^3$, and $\hat{V} \in \mathbb{R}^3$ denote the estimates of attitude, position, and linear velocity, respectively. Define the errors between the true and the estimated values of attitude ($\tilde{R}$), position ($\tilde{P}$), and linear velocity ($\tilde{V}$) as follows:

$$\begin{cases} \tilde{R} = R\hat{R}^\top \\ \tilde{P} = P - \hat{P} \\ \tilde{V} = V - \hat{V} \end{cases} \tag{31}$$

Let $\hat{\sigma}$ be the upper bound covariance estimate of σ and define the estimation error as

$$\tilde{\sigma} = \sigma - \hat{\sigma} \in \mathbb{R}^3 \tag{32}$$

For attitude estimation, our objective is to utilize direct vector observations and measurements in the implementation. As such, from (19), define

$$M_r = \sum_{i=1}^{3} s_i r_i r_i^\top, \quad M_B = \sum_{i=1}^{3} s_i v_i v_i^\top \tag{33}$$

where s_i denotes the ith sensor confidence such that $\sum_{i=1}^{3} s_i = 3$. Define

$$\hat{v}_i = \hat{R}^\top r_i, \quad \forall i = 1, 2, 3 \tag{34}$$

Therefore, one finds

$$\begin{aligned} \mathbf{vex}(\boldsymbol{\mathcal{P}}_a(M_r\tilde{R})) &= \frac{1}{2}\mathbf{vex}(M_r\tilde{R} - \tilde{R}^\top M_r) \\ &= \frac{1}{2}\mathbf{vex}\left(\sum_{i=1}^{3} s_i r_i v_i^\top \hat{R}^\top - \sum_{i=1}^{3} s_i \hat{R} v_i r_i^\top\right) \\ &= \frac{1}{2}\sum_{i=1}^{3}\hat{R}s_i(v_i \times \hat{v}_i) \end{aligned} \tag{35}$$

where $[v_i \times \hat{v}_i]_\times = \hat{v}_i v_i^\top - v_i\hat{v}_i^\top$. Also, one shows

$$\begin{aligned} E_r &= ||M_r\tilde{R}||_{\mathrm{I}} = \frac{1}{4}\mathrm{Tr}\{M_r(\mathbf{I}_3 - \tilde{R})\} \\ &= \frac{1}{4}\mathrm{Tr}\left\{M_r - \sum_{i=1}^{3} s_i\hat{R}\hat{v}_i v_i^\top\hat{R}^\top\right\} \end{aligned} \tag{36}$$

where $E_r : \mathbb{SO}(3) \to \mathbb{R}_+$ with $E_r > 0 \forall \tilde{R} \neq \mathbf{I}_3$ and $E_r = 0$ at $\tilde{R} = \mathbf{I}_3$. To this end, let P_y denote a reconstructed position satisfying Assumption 1 which can be obtained, for instance, as follows:

$$\begin{cases} P_y = (A^\top A)^{-1}A^\top B, & \text{TOA} \\ \overline{P}_y = \begin{bmatrix} P_y \\ ||P_y - h_1|| \end{bmatrix} = (A^\top A)^{-1}A^\top B, & \text{TDOA} \end{cases} \tag{37}$$

where A and B matrices are defined in Section III. Let us define the following set of equations which includes a covariance adaptation mechanism and correction factors:

$$\begin{cases} E_r = \frac{1}{4}\mathrm{Tr}\sum_{i=1}^{3} s_i(r_i r_i^\top - \hat{R}\hat{v}_i v_i^\top\hat{R}^\top) \\ \mathcal{D}_v = \mathrm{diag}(\sum_{i=1}^{3} s_i v_i \times \hat{v}_i) \\ \dot{\hat{\sigma}} = \gamma_\sigma\frac{E_r + 2}{8}\exp(E_r)\mathcal{D}_\mathrm{v}(\sum_{i=1}^{n} s_i v_i \times \hat{v}_i) - k_\sigma\gamma_\sigma\hat{\sigma} \\ w_\Omega = -\frac{k_1}{2}\sum_{i=1}^{n}\hat{R}s_i(v_i \times \hat{v}_i) - \frac{1}{8}\frac{E_r + 2}{E_r + 1}\hat{R}\mathcal{D}_\mathrm{v}\hat{\sigma} \\ w_V = -\frac{k_v}{\varepsilon}(P_y - \hat{P}) - [w_\Omega]_\times\hat{P} \\ w_a = -k_a(P_y - \hat{P}) - [w_\Omega]_\times\hat{V} \end{cases} \tag{38}$$

where γ_σ, k_1, k_v, k_a, ε, and k_σ are positive constants. Now let us propose the following navigation stochastic filter design:

$$\begin{cases} \dot{\hat{R}} = \hat{R}[\Omega_m]_\times - [w_\Omega]_\times\hat{R} \\ \dot{\hat{P}} = \hat{V} - [w_\Omega]_\times\hat{P} - w_V \\ \dot{\hat{V}} = \hat{R}a_m + \overrightarrow{\mathtt{g}} - [w_\Omega]_\times\hat{V} - w_a, \end{cases} \quad \underbrace{\dot{\hat{X}} = \hat{X}U_m - W\hat{X}}_{\text{Compact form}} \tag{39}$$

Quaternion form of the stochastic filter design proposed above is outlined in the Appendix. For the compact form, $\hat{X} \in \mathbb{SE}_2(3)$ describes the estimate of X, $U_m = u([\Omega_m]_\times, 0_{3\times 1}, a_m, 1) \in \mathcal{U}_\mathcal{M}$, and $W = u([w_\Omega]_\times, w_V, w_a, 1) \in \mathcal{U}_\mathcal{M}$, refer to the map in (4). For simplicity's sake, in the analysis, $P = P_y$.

Theorem 1: Recall the nonlinear stochastic differential system in (22). Consider that at each time instant, at least 3 non-collinear measurements/observations as to (19) are available also consider Assumption 1 holds true (for any of TOA- or TDOA-based approaches). Let the nonlinear navigation stochastic differential estimator in (39) be integrated with the direct measurements and innovation terms in (37) and (38) such that $\Omega_m = \Omega + n_\Omega$ and $a_m = a + n_a$. Thus, all the closed-loop signals are almost semi-globally uniformly ultimately bounded in the mean square.

Proof: From (22), (36), (31), and (39), one obtains

$$\begin{aligned}\frac{d}{dt}E_r &= \frac{d}{dt}\frac{1}{4}\mathrm{Tr}\{M_r(\mathbf{I}_3 - \tilde{R})\}\\ &= -\frac{1}{4}\mathrm{Tr}\{M_r\tilde{R}[w_\Omega]_\times\} + \frac{1}{4}\mathrm{Tr}\{M_r\tilde{R}[\hat{R}\mathcal{Q}_\Omega d\beta_\Omega]_\times\}\\ &= \frac{1}{2}\mathbf{vex}(\boldsymbol{\mathcal{P}}_a(M_r\tilde{R}))^\top(w_\Omega dt - \hat{R}\mathcal{Q}_\Omega d\beta_\Omega) \end{aligned} \tag{40}$$

Note that M_r is a constant matrix and $\mathrm{Tr}\{M_r\tilde{R}[w_\Omega]_\times\} = \mathrm{Tr}\{\boldsymbol{\mathcal{P}}_a(M_r\tilde{R})[w_\Omega]_\times\} = -\frac{1}{2}\mathbf{vex}(\boldsymbol{\mathcal{P}}_a(M_r\tilde{R}))^\top w_\Omega$. From (22), (31), and (39), one shows

$$\begin{cases}\dot{\tilde{P}} = \tilde{V} + [w_\Omega]_\times\hat{P} + w_V\\ d\tilde{V} = ((\tilde{R} - \mathbf{I}_3)\hat{R}a + [w_\Omega]_\times\hat{V} + w_a)dt - R\mathcal{Q}d\beta_a\end{cases} \tag{41}$$

Define $\mathbb{U}_T = \mathbb{U}_T(E_r, \tilde{P}, \tilde{V}, \tilde{\sigma})$ as a Lyapunov function candidate such that

$$\mathbb{U}_T = \mathbb{U}_R + \mathbb{U}_{PV} \tag{42}$$

where $\mathbb{U}_T : \mathbb{SO}(3) \times \mathbb{R}^3 \times \mathbb{R}^3 \times \mathbb{R}^3 \to \mathbb{R}_+$. Now consider the following Lyapunov function candidate $\mathbb{U}_R : \mathbb{SO}(3) \times \mathbb{R}^3 \to \mathbb{R}_+$:

$$\mathbb{U}_R = \exp(E_r)E_r + \frac{1}{2\gamma_\sigma}||\tilde{\sigma}||^2 \tag{43}$$

From (25), one can show that $\frac{\partial}{\partial E_r}\mathbb{U}_R = \exp(E_r)(E_r + 1)$ and $\frac{\partial^2}{\partial E_r^2}\mathbb{U}_R = \exp(E_r)(E_r + 2)$. From (27) and (39), one obtains

$$\begin{aligned}\mathcal{L}\mathbb{U}_R &= \left(\frac{\partial\mathbb{U}_R}{\partial E_r}\right)^\top f_R + \frac{1}{2}\mathrm{Tr}\left\{g_R\mathcal{Q}_\Omega^2 g_R^\top\frac{\partial^2\mathbb{U}_R}{\partial e_R^2}\right\} - \frac{1}{\gamma_\sigma}\tilde{\sigma}^\top\dot{\hat{\sigma}}\\ &= \frac{1}{8}\frac{\partial^2 U_R}{\partial E_r^2}\mathbf{vex}(\boldsymbol{\mathcal{P}}_a(M_r\tilde{R}))^\top\hat{R}\mathcal{Q}_\Omega^2\hat{R}^\top\mathbf{vex}(\boldsymbol{\mathcal{P}}_a(M_r\tilde{R}))\\ &\quad + \frac{1}{2}\frac{\partial^2 U_R}{\partial E_r^2}\mathbf{vex}(\boldsymbol{\mathcal{P}}_a(M_r\tilde{R}))^\top w_\Omega - \frac{1}{\gamma_\sigma}\tilde{\sigma}^\top\dot{\hat{\sigma}} \end{aligned} \tag{44}$$

where $||\mathcal{Q}^2||_F \leq ||\mathrm{diag}(\sigma)||_F$ as in (24). Substituting $\dot{\hat{\sigma}}$ and w_Ω with their definitions in (38) and in view of (29) in Lemma 2, it becomes apparent that

$$\begin{aligned}\mathcal{L}\mathbb{U}_R &\leq -(1 + \mathrm{Tr}\{\tilde{R}\})\frac{k_1\underline{\lambda_{\overline{M_r}}}}{4}\exp(E_r)E_r + k_\sigma\tilde{\sigma}^\top\hat{\sigma}\\ &\leq -k_1c_R||M_r\tilde{R}||_{\mathrm{I}} - \frac{k_\sigma}{2}||\tilde{\sigma}||^2 + \frac{k_\sigma}{2}||\sigma||^2\end{aligned} \tag{45}$$

with $k_\sigma\tilde{\sigma}^\top\sigma \leq \frac{k_\sigma}{2}||\sigma||^2 + \frac{k_\sigma}{2}||\tilde{\sigma}||^2$ (see Young's inequality) and $c_R = \frac{1}{4}\underline{\lambda}_{\overline{M_r}}(1 + \mathrm{Tr}\{\tilde{R}\})$. Define $\underline{\lambda}_R = \min\{k_1c_R, \frac{k_\sigma}{2}\}$ and $e_R = [||M_r\tilde{R}||_{\mathrm{I}}, ||\tilde{\sigma}||]^\top$. Thus, $\mathcal{L}\mathbb{U}_R$ can be described as

$$\mathcal{L}\mathbb{U}_R \leq -\underline{\lambda}_R||e_R||^2 + \frac{k_\sigma}{2}||\sigma||^2 \tag{46}$$

Consider the following real-valued function $\mathbb{U}_{PV} : \mathbb{R}^3 \times \mathbb{R}^3 \to \mathbb{R}_+$:

$$\mathbb{U}_{PV} = \frac{1}{4}||\tilde{P}||^4 + \frac{1}{4k_d}||\tilde{V}||^4 - \frac{1}{3\mu}||\tilde{V}||^2\tilde{V}^\top\tilde{P} \tag{47}$$

with k_d and μ being positive constants. Hence, one obtains

$$\begin{aligned}\frac{\partial\mathbb{U}_{PV}}{\partial\tilde{P}} &= ||\tilde{P}||^2\tilde{P} - \frac{1}{3\mu}||\tilde{V}||^2\tilde{V}\\ \frac{\partial\mathbb{U}_{PV}}{\partial\tilde{V}} &= \frac{1}{k_d}||\tilde{V}||^2\tilde{V} - \frac{1}{\mu}||\tilde{V}||^2\tilde{P}\\ \frac{\partial^2\mathbb{U}_{PV}}{\partial\tilde{V}^2} &= \frac{1}{k_d}(||\tilde{V}||^2\mathbf{I}_3 + 2\tilde{V}\tilde{V}^\top - 2\tilde{P}\tilde{V}^\top)\end{aligned} \tag{48}$$

Recall that $\mathrm{Tr}\{\hat{R}\mathcal{Q}^2\hat{R}^\top\} = \mathrm{Tr}\{\mathcal{Q}^2\}$, $\tilde{V}^\top[w_\Omega]_\times\tilde{V} = 0$, and $||\mathbf{I}_3 - \tilde{R}||_F = 2\sqrt{2}\sqrt{||\tilde{R}||_{\mathrm{I}}} \leq 4\overline{\lambda}_M\sqrt{||M\tilde{R}||_{\mathrm{I}}}$ (see [21]). As such, in view of (27), (41), (47), and (48), one finds

$$\begin{aligned}&\mathcal{L}\mathbb{U}_{PV}\\ &= (||\tilde{P}||^2\tilde{P} - \frac{1}{3\mu}||\tilde{V}||^2\tilde{V})^\top(\tilde{V} + [w_\Omega]_\times\hat{P} + w_V)\\ &\quad + ||\tilde{V}||^2(\frac{1}{k_d}\tilde{V} - \frac{1}{\mu}\tilde{P})^\top((\tilde{R} - \mathbf{I}_3)\hat{R}a + [w_\Omega]_\times\hat{V} + w_a)\\ &\quad + \frac{1}{2k_d}\mathrm{Tr}\left\{(||\tilde{V}||^2\mathbf{I}_3 + 2\tilde{V}\tilde{V}^\top - 2\tilde{P}\tilde{V}^\top)R\mathcal{Q}^2R^\top\right\}\\ &\leq -c_1||\tilde{P}||^4 - c_2||\tilde{V}||^4 + c_3||\tilde{V}||^2||\tilde{P}||^2\\ &\quad + 2c_g||\tilde{V}||^2\sqrt{||M\tilde{R}||_{\mathrm{I}}} + \frac{1}{4k_d}||\sigma||^2\end{aligned} \tag{49}$$

where $c_m = \max\{3\mu k_d, 3\mu, 6k_d\mu\overline{\lambda}_M c_a, 6k_d k_a\}$, $c_a = \sup_{t\geq 0}||a||$, $c_1 = \frac{2k_v - \varepsilon}{2\varepsilon}$, $c_2 = \frac{k_d - 4\mu}{3\mu k_d}$, $c_3 = (\varepsilon c_m + k_v k_d)/\varepsilon k_d\mu$, and $c_g = \max\{\frac{4\overline{\lambda}_M||a||}{k_d}, \frac{4\overline{\lambda}_M||a||}{\mu}\}$. Therefore, $\mathcal{L}\mathbb{U}_{PV}$ in (49) becomes

$$\begin{aligned}\mathcal{L}\mathbb{U}_{PV} &\leq -e_{PV}^\top\underbrace{\begin{bmatrix} c_1 & -\frac{c_3}{2}\\ -\frac{c_3}{2} & c_2\end{bmatrix}}_{Q_{PV}}e_{PV}\\ &\quad + 2c_g||e_{PV}||\,||e_R|| + \frac{1}{4k_d}||\sigma||^2\end{aligned} \tag{50}$$

where $e_{PV} = [||\tilde{P}||^2, ||\tilde{V}||^2]^\top$. Q_{PV} is made positive by selecting $k_v > \varepsilon/2$, $k_d > 4\mu$, and $c_1c_2 > \frac{c_3^2}{4}$. Let us define $\underline{\lambda}_{PV} = \underline{\lambda}(Q_{PV})$. From (42), (46), and (50), the differential operator $\mathcal{L}\mathbb{U}_R$ and $\mathcal{L}\mathbb{U}_{PV}$ can be combined and $\mathcal{L}\mathbb{U}_T$ can be expressed as

$$\begin{aligned}\mathcal{L}\mathbb{U}_T &\leq -\underline{\lambda}_R||e_R||^2 - \underline{\lambda}_{PV}||e_{PV}||^2 + 2c_g||e_{PV}||\,||e_R||\\ &\quad + (\frac{1}{4k_d} + \frac{k_\sigma}{2})||\sigma||^2\\ \mathcal{L}\mathbb{U}_T &\leq -e_T^\top\underbrace{\begin{bmatrix}\underline{\lambda}_R & -c_g\\ -c_g & \underline{\lambda}_{PV}\end{bmatrix}}_{Q_T}e_T + \eta_\sigma\end{aligned} \tag{51}$$

where $\eta_\sigma = (\frac{1}{4k_d} + \frac{k_\sigma}{2})||\sigma||^2$ and $e_T = [||e_R||, ||e_{PV}||]^\top$. Hence, Q_T is made positive by selecting $\underline{\lambda}_R > \frac{c_g^2}{4\underline{\lambda}_{PV}}$. Let us define $\underline{\lambda}_T = \underline{\lambda}(Q_T)$. Hence, from (51), one shows

$$\mathcal{L}\mathbb{U}_T \leq -\underline{\lambda}_T||e_T||^2 + \eta_\sigma \tag{52}$$

In other words

$$d\mathbb{E}[\mathbb{U}_T]/dt = \mathbb{E}[\mathcal{L}\mathbb{U}_T] \leq -\underline{\lambda}_T\mathbb{E}[\mathbb{U}_T] + \eta_\sigma \tag{53}$$

In view of Lemma 1, it is obvious that

$$0 \leq \mathbb{E}[\mathbb{U}_T(t)] \leq \mathbb{U}_T(0)\exp(-\underline{\lambda}_T t) + \eta_\sigma/\underline{\lambda}_T$$

Thereby, it becomes apparent that e_T or $(||M\tilde{R}||_{\mathrm{I}}, ||\tilde{P}||, ||\tilde{V}||, ||\tilde{\sigma}||)$ is almost SGUUB completing the proof. ∎

A. Discrete Implementation

Define Δt as a small sample time. Algorithm 1 details the implementation steps of the proposed continuous nonlinear stochastic navigation filter (37)-(39) but in a discrete form. $\exp(\cdot)$ in Algorithm 1 refers to an exponential of a matrix, commonly termed "expm". In the algorithm, the subscript k denotes the kth iteration.

V. Pose Determination From UWB

The UWB industry is challenged with improving ranging accuracy. Improved UWB ranging accuracy will constitute a breakthrough enabling pose (orientation + position) determination based solely on UWB anchors and tags. This will alleviate the need for a typical 9-axis IMU (gyroscope + accelerometer + magnetometer). Many vehicles (e.g., mobile robots and drones) are equipped with a 6-axis IMU (gyroscope + accelerometer). Thereby, obtaining an additional observation and measurement for orientation determination requires equipping the vehicle with an additional motion sensor such as a magnetometer to improve the attitude estimation accuracy. Another approach suggests equipping the vehicle with a vision unit (e.g., monocular or stereo camera) to enhance orientation and positioning accuracy [1], [2], [6]. However, adding a vision unit increases the computational cost (e.g., feature extraction and pose estimation) and places additional load on the battery power consumption. Considering the advantages offered by the UWB technology, such as robustness against multipath interference and fading [24], [25], localization in LOS and NLOS [32], and low cost and power requirements [15], [16], improving UWB ranging accuracy will significantly advance the area of autonomous mobility and intelligent transportation. Orientation and position of a vehicle equipped with IMU and high accuracy UWB navigating in 3D space can be fully defined if one of the following conditions is satisfied:

(i) 9-axis IMU, UWB anchors satisfying Assumption 1, and a vehicle equipped with at least one tag.
(ii) 6-axis IMU, UWB anchors satisfying Assumption 1, and a vehicle equipped with at least two tags.
(iii) Gyroscope, UWB anchors satisfying Assumption 1, and a vehicle equipped with at least three tags.

The problem formulation in Section III and the filter design in IV consider that UWB anchors satisfy Assumption 1 such that the UWB tag enables vehicle positioning and a 9-axis IMU enables orientation determination (as detailed in Theorem 1) which shows (i). Fig. 3 illustrates a system with two tags placed at a considerable distance and a 6-axis IMU capable of full pose determination. Let $P = [x, y, z]^\top$ denote the vehicle's position (at the center point) which also represents the position between $\{\mathcal{B}\}$-frame and $\{\mathcal{I}\}$-frame. Assume that two UWB tags are placed at the vehicle's edges as illustrated in Fig. 3 $G_1 = [x_{g1}, y_{g1}, z_{g1}]^\top$ and $G_2 = [x_{g2}, y_{g2}, z_{g2}]^\top$ are described with respect to the $\{\mathcal{I}\}$-frame such that $P = \frac{1}{2}(G_1 + G_2)$. In view of Assumption 1, the position of each tag can be easily defined. The transformation from G_1 to P or from G_2 to P can be obtained using vehicle's orientation R and a coordination vector $s_1 = [x_{s1}, y_{s1}, z_{s1}]^\top$. s_1 is a known constant vector, and can be initially calculated given known orientation (e.g., positioning the vehicle $\{\mathcal{B}\}$-frame at the $\{\mathcal{I}\}$-frame). As such, one obtains $G_1 = P + Rs_1$ or $G_2 = P - Rs_1$. Given 6-axis IMU and two tags, the necessary 3 observations

---

Algorithm 1 Discrete Navigation Stochastic Filter

Initialization:

1: Set $\hat{P}_{0|0}, \hat{V}_{0|0}, \hat{\sigma}_0 \in \mathbb{R}^3$ and $\hat{R}_{0|0} \in \mathbb{SO}(3)$.

2: Set $k = 0$ and pick the filter design parameters.

while (1) **do**

/* Prediction */

3: $$\hat{X}_{k|k} = \begin{bmatrix} \hat{R}_{k|k} & \hat{P}_{k|k} & \hat{V}_{k|k} \\ 0_{1\times 3} & 1 & 0 \\ 0_{1\times 3} & 0 & 1 \end{bmatrix} \in \mathbb{SE}_2(3) \text{ and}$$
$$\hat{U}_k = \begin{bmatrix} [\Omega_m[k]]_\times & 0_{3\times 1} & a_m[k] \\ 0_{1\times 3} & 0 & 0 \\ 0_{1\times 3} & 1 & 0 \end{bmatrix} \in \mathcal{U}_{\mathcal{M}}$$

4: $\hat{X}_{k+1|k} = \hat{X}_{k|k}\exp(\hat{U}_k \Delta t)$

/* Update step */

5: $$\begin{cases} P_y = (A^\top A)^{-1}A^\top B, & \text{TOA} \\ \overline{P}_y = \begin{bmatrix} P_y \\ ||P - h_1|| \end{bmatrix} = (A^\top A)^{-1}A^\top B, & \text{TDOA} \end{cases}$$

6: $$\begin{cases} v_1 = \dfrac{a_m}{||a_m||}, & r_1 = \dfrac{-\overrightarrow{\mathtt{g}}}{||-\overrightarrow{\mathtt{g}}||} \\ v_2 = \dfrac{m_m}{||m_m||}, & r_2 = \dfrac{m_r}{||m_r||} \\ v_3 = \dfrac{v_1 \times v_2}{||v_1 \times v_2||}, & r_3 = \dfrac{r_1 \times r_2}{||r_1 \times r_2||} \end{cases}$$

7: $$\begin{cases} E_r &= \dfrac{1}{4}\mathrm{Tr}\displaystyle\sum_{i=1}^{3} s_i(r_i r_i^\top - \hat{R}_{k|k}\hat{v}_i v_i^\top \hat{R}_{k|k}^\top) \\ \mathcal{D}_v &= \mathrm{diag}(\displaystyle\sum_{i=1}^{3} s_i v_i \times \hat{v}_i) \end{cases}$$

8: $$\begin{cases} \hat{\sigma}_{k+1} &= \hat{\sigma}_k - \Delta t k_\sigma \gamma_\sigma \hat{\sigma}_k \\ &\quad + \Delta t \gamma_\sigma \dfrac{E_r + 2}{8}\exp(E_r)\mathcal{D}_v(\displaystyle\sum_{i=1}^{n} s_i v_i \times \hat{v}_i) \\ w_\Omega &= -\dfrac{k_1}{2}\displaystyle\sum_{i=1}^{n}\hat{R}s_i(v_i \times \hat{v}_i) - \dfrac{1}{8}\dfrac{E_r + 2}{E_r + 1}\hat{R}\mathcal{D}_v\hat{\sigma}_k \\ w_V &= -\dfrac{k_v}{\varepsilon}(P_y - \hat{P}_{k|k}) - [w_\Omega]_\times \hat{P}_{k|k} \\ w_a &= -\overrightarrow{\mathtt{g}} - k_a(P_y - \hat{P}_{k|k}) - [w_\Omega]_\times \hat{V}_{k|k} \end{cases}$$

9: $$W_k = \begin{bmatrix} [w_\Omega[k]]_\times & w_V[k] & w_a[k] \\ 0_{1\times 3} & 0 & 0 \\ 0_{1\times 3} & 1 & 0 \end{bmatrix}$$

10: $\hat{X}_{k+1|k+1} = \exp(-W_k \Delta t)\hat{X}_{k+1|k}$

11: $k = k + 1$

end while

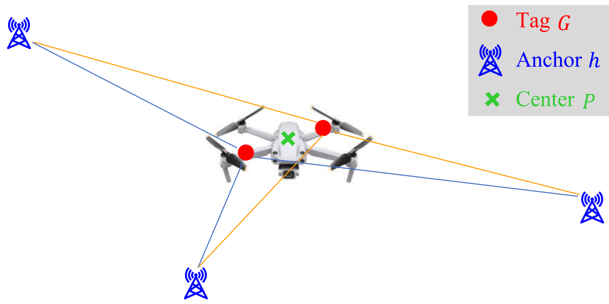

Fig. 3. Multiple tag placement for pose (orientation + position) determination.

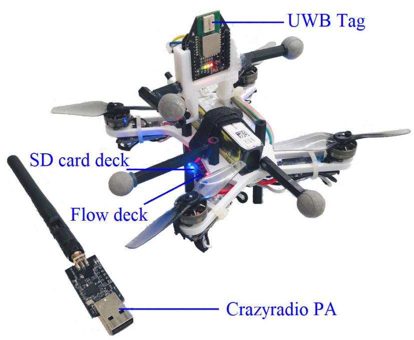

Fig. 4. Customized drone with a flight controller [33].

and measurements can be obtained as follows:

$$\begin{cases} a_m \approx -R^\top \overrightarrow{g}, & \text{accelerometer} \\ s_1 = R^\top (G_1 - P) & \\ s_2 = \dfrac{a_m \times s_1}{||a_m \times s_1||}, & r_3 = \dfrac{-\overrightarrow{g} \times (G_1 - P)}{||-\overrightarrow{g} \times (G_1 - P)||} \end{cases} \tag{54}$$

In view of the above discussion, UWB anchors satisfying Assumption 1 can position the vehicle. Anchors and three tags noncollinearly placed on the vehicle are sufficient to formulate three equations for vehicle coordination analogously to (54) without the need for a magnetometer or an accelerometer.

VI. Validation

This section illustrates the robustness of the proposed nonlinear stochastic filter for inertial navigation based on the fusion of UWB and IMU sensors. We have used the publicly available real-world drone flight dataset published by Zhao et al., 2022 [33]. The dataset includes measurements obtained from a drone equipped with one UWB tag and a 6-axis IMU (see Fig. 4). 8 fixed UWB anchors were present during the drone flight (satisfying Assumption 1). Additionally, the dataset supplies ground truth information (true drone's position and orientation described with respect to unit-quaternion).

The linear velocity is not provided in the dataset. Therefore, a classical maximum likelihood (ML) method has been utilized to identify the true linear velocity (for the purpose of comparison) [34], [35]. To test the filter convergence capability against large error initialization, we initiated the drone flight at its true original position provided in the dataset $P(0) = [-0.061, 1.244, 1.506]^\top$ and a linear velocity $V(0) = [-0.4708, 0.1308, -0.3363]^\top$, while the estimated initial position and linear velocity were set as $\hat{P}(0) = [-2, -3, 0]^\top$ and $\hat{V}(0) = [0, 0, 0]^\top$, respectively. The UWB tag is not positioned at the vehicle's center. As such, in order to adjust the UWB tag's position to the vehicle's center a translation vector $v_c = [-0.012, 0.001, 0.091]^\top m$ [33], the ranging distance is calculated by:

$$d_{i,j} = ||R v_c + P - h_j|| - ||R v_c + P - h_i|| \tag{55}$$

where $d_{i,j}$ denotes the TDOA range distance, R refers to the drone's orientation, P stands for the drone's position, and h_j denotes the jth anchor position (see Section III-B). The expression in (55) has been utilized for obtaining the reconstructed position P_y described in (15). To include a magnetometer, we set $m_r = [-1.3, 0, 1.5]^\top$ and calculated $m_m = R^\top m_r + n_m$ where $n_m = \mathcal{N}(0, 0.2)$ refers to a normally distributed random noise vector with a zero mean and a standard deviation of 0.2. The design parameters have been

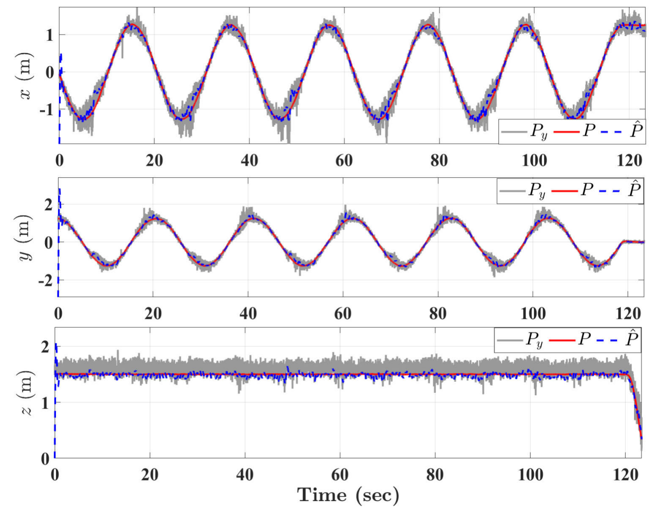

Fig. 5. Trial Const1 [33]: The true drone's position P is marked as a red solid line, the estimated position $\hat{P}$ (proposed) is plotted as a blue dash line, and the reconstructed position P_y is presented as a gray solid line.

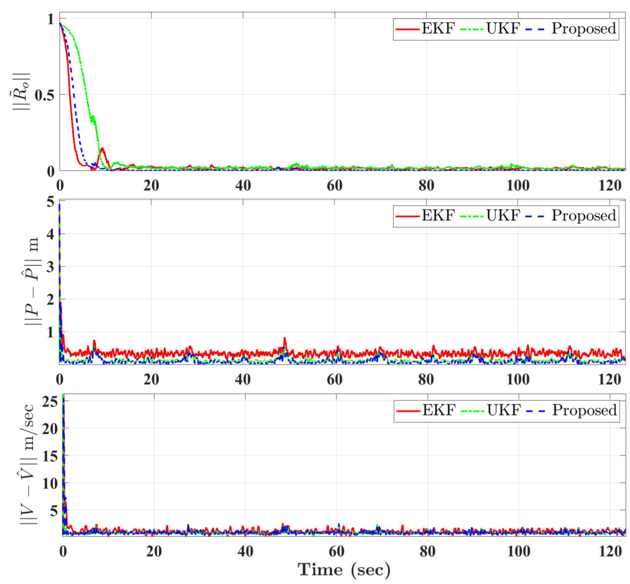

Fig. 6. Error convergence: Nonlinear stochastic filter (proposed) plotted as a blue dash line vs EKF and UKF.

selected as follows: $k_1 = 3$, $k_v = 3$, $k_a = 7$, $\gamma_s = 0.1$, $\varepsilon = 0.5$, and $k_\sigma = 0.1$ where the initial covariance estimate has been set to $\hat{\sigma}(0) = [0, 0, 0]^\top$. The TDOA of UWB measurements and IMU data were collected at a rate of 500 Hz. Therefore, to confirm robustness of the proposed filter, the algorithm was implemented at a lower sampling rate (100 Hz) with $\Delta T = 0.01$ sec.

The experimental validation uses "Const1-Trial" of the UTIL dataset [33]. Fig. 5 illustrates the true drone's position P marked as a red solid line, the estimated position $\hat{P}$ plotted as a blue dash line, and the reconstructed position P_y in gray color obtained using $d_{i,j}$ TDOA range distance, fixed anchors (h_i for $i = 1, 2 \ldots, 8$), and v_c described in (55). The reconstructed position P_y in Fig. 5 demonstrates a high level of noise attached to measurements. Despite the high level of measurement uncertainties, Fig. 5 reveals highly accurate estimation of the vehicle's position in 3D space. Furthermore, Fig. 6 illustrates in blue the successful and rapid error convergence of the proposed filter in terms of orientation $||\tilde{R}||_{\rm I} = \frac{1}{4}{\rm Tr}\{\mathbf{I}_3 - \hat{R}R^\top\}$, position $||P - \hat{P}||$, and linear velocity $||V - \hat{V}||$ from large error initialization to the neighborhood of the origin. Additionally, Fig. 6 compares the performance of the proposed stochastic filter against EKF and UKF. As has been illustrated in Fig. 6, UKF is slower in orientation convergence than the proposed stochastic nonlinear filter. At steady-state, UKF shows more oscillatory behavior when compared to the EKF, and EKF presents more oscillatory behavior than the proposed nonlinear stochastic filter.

VII. Conclusion

A novel nonlinear stochastic filter for inertial navigation on the Lie Group of $\mathbb{SE}_2(3)$ is proposed to estimate the vehicle's attitude, position, and linear velocity. The proposed filter utilizes the direct measurements supplied by UWB and IMU achieving semi-globally uniformly ultimately bounded (SGUUB) stability of the closed loop error signals. The filter effectively tackles IMU uncertainties and ensures noise attenuation. The necessary conditions for orientation and position determination have been outlined considering IMU and UWB fusion or the exclusive use of UWB technology. The validation performed using a real-world unmanned aerial vehicle flight dataset has revealed the capability of the discrete form of the proposed approach to produce accurate estimates of orientation, position, and linear velocity.

Appendix
Quaternion Representation of Navigation Filter

Let $Q = [q_0, q^\top]^\top \in \mathbb{S}^3$ refer to a unit-quaternion vector with $q_0 \in \mathbb{R}$ and $q \in \mathbb{R}^3$, and the 3-sphere group $\mathbb{S}^3$ be defined by

$$\mathbb{S}^3 = \{Q \in \mathbb{R}^4 \Big| \, ||Q|| = \sqrt{q_0^2 + q^\top q} = 1\}$$

$\mathbb{SO}(3)$ can be obtained from unit-quaternion through the following map $\mathcal{R}_Q : \mathbb{S}^3 \to \mathbb{SO}(3)$:

$$\mathcal{R}_Q = (q_0^2 - ||q||^2)\mathbf{I}_3 + 2qq^\top + 2q_0\left[q\right]_\times \in \mathbb{SO}(3) \tag{56}$$

Let $\hat{Q} = [\hat{q}_0, \hat{q}^\top]^\top \in \mathbb{S}^3$ denote the estimate of $Q = [q_0, q^\top]^\top \in \mathbb{S}^3$ and the attitude estimate from quaternion estimate be given by

$$\hat{\mathcal{R}}_Q = (\hat{q}_0^2 - ||\hat{q}||^2)\mathbf{I}_3 + 2\hat{q}\hat{q}^\top + 2\hat{q}_0\left[\hat{q}\right]_\times \in \mathbb{SO}(3)$$

Similar to (37), let us obtain the vehicle position as follows:

$$\begin{cases} P_y = (A^\top A)^{-1}A^\top B, & \text{TOA} \\ \overline{P}_y = \begin{bmatrix} P_y \\ ||P - h_1|| \end{bmatrix} = (A^\top A)^{-1}A^\top B, & \text{TDOA} \end{cases} \tag{57}$$

Consider the covariance adaptation mechanism and the correction factors using the following set of equations:

$$\begin{cases} E_r = \frac{1}{4}{\rm Tr}\sum_{i=1}^{3} s_i(r_i r_i^\top - \hat{\mathcal{R}}_Q \hat{v}_i v_i^\top \hat{\mathcal{R}}_Q^\top) \\ \mathcal{D}_v = {\rm diag}(\sum_{i=1}^{3} s_i v_i \times \hat{v}_i) \\ \dot{\hat{\sigma}} = \gamma_\sigma \frac{E_r + 2}{8}\exp(E_r)\mathcal{D}_{\rm v}(\sum_{i=1}^{n} s_i v_i \times \hat{v}_i) - k_\sigma \gamma_\sigma \hat{\sigma} \\ w_\Omega = -\frac{k_1}{2}\sum_{i=1}^{n} \hat{\mathcal{R}}_Q s_i(v_i \times \hat{v}_i) - \frac{1}{8}\frac{E_r + 2}{E_r + 1}\hat{\mathcal{R}}_Q \mathcal{D}_{\rm v}\hat{\sigma} \\ w_V = -\frac{k_v}{\varepsilon}(P_y - \hat{P}) - [w_\Omega]_\times \hat{P} \\ w_a = -k_a(P_y - \hat{P}) - [w_\Omega]_\times \hat{V} \end{cases} \tag{58}$$

Consider the navigation stochastic filter kinematics as follows:

$$\begin{cases} \Theta_m = \begin{bmatrix} 0 & -\Omega_m^\top \\ \Omega_m & -[\Omega_m]_\times \end{bmatrix}, \quad \Psi = \begin{bmatrix} 0 & -w_\Omega^\top \\ w_\Omega & [w_\Omega]_\times \end{bmatrix} \\ \dot{\hat{Q}} = \frac{1}{2}\Theta_m \hat{Q} - \frac{1}{2}\Psi \hat{Q} \\ \dot{\hat{P}} = \hat{V} - [w_\Omega]_\times \hat{P} - w_V \\ \dot{\hat{V}} = \hat{\mathcal{R}} a_m + \overrightarrow{\mathtt{g}} - [w_\Omega]_\times \hat{V} - w_a \end{cases} \tag{59}$$

References

[1] A. Beauvisage, K. Ahiska, and N. Aouf, "Robust multispectral visual-inertial navigation with visual odometry failure recovery," *IEEE Trans. Intell. Transp. Syst.*, vol. 23, no. 7, pp. 9089–9101, Jul. 2022.

[2] H. A. Hashim, M. Abouheaf, and M. A. Abido, "Geometric stochastic filter with guaranteed performance for autonomous navigation based on IMU and feature sensor fusion," *Control Eng. Pract.*, vol. 116, Nov. 2021, Art. no. 104926.

[3] Q. Zou, Q. Sun, L. Chen, B. Nie, and Q. Li, "A comparative analysis of LiDAR SLAM-based indoor navigation for autonomous vehicles," *IEEE Trans. Intell. Transp. Syst.*, vol. 23, no. 7, pp. 6907–6921, Jul. 2022.

[4] Z. Liu, Y. Li, Y. Wu, and S. He, "Formation control of nonholonomic unmanned ground vehicles via unscented Kalman filter-based sensor fusion approach," *ISA Trans.*, vol. 125, pp. 60–71, Jun. 2022.

[5] E. D'Amato, M. Mattei, I. Notaro, and V. Scordamaglia, "UAV sensor FDI in duplex attitude estimation architectures using a set-based approach," *IEEE Trans. Instrum. Meas.*, vol. 67, no. 10, pp. 2465–2475, Oct. 2018.

[6] J. Cheng, L. Yang, Y. Li, and W. Zhang, "Seamless outdoor/indoor navigation with WiFi/GPS aided low cost inertial navigation system," *Phys. Commun.*, vol. 13, pp. 31–43, Dec. 2014.

[7] H. A. Hashim, A. E. E. Eltoukhy, and A. Odry, "Observer-based controller for VTOL-UAVs tracking using direct vision-aided inertial navigation measurements," *ISA Trans.*, vol. 137, pp. 133–143, Jun. 2023.

[8] Q. Tian, K. I. Wang, and Z. Salcic, "A resetting approach for INS and UWB sensor fusion using particle filter for pedestrian tracking," *IEEE Trans. Instrum. Meas.*, vol. 69, no. 8, pp. 5914–5921, Aug. 2020.

[9] J. Xiong, J. W. Cheong, Z. Xiong, A. G. Dempster, S. Tian, and R. Wang, "Adaptive hybrid robust filter for multi-sensor relative navigation system," *IEEE Trans. Intell. Transp. Syst.*, vol. 23, no. 8, pp. 11026–11040, Aug. 2022.

[10] N. Dwek et al., "Improving the accuracy and robustness of ultra-wideband localization through sensor fusion and outlier detection," *IEEE Robot. Autom. Lett.*, vol. 5, no. 1, pp. 32–39, Jan. 2020.

[11] K. Guo, X. Li, and L. Xie, "Ultra-wideband and odometry-based cooperative relative localization with application to multi-UAV formation control," *IEEE Trans. Cybern.*, vol. 50, no. 6, pp. 2590–2603, Jun. 2020.

[12] Y. Shen, H. Wymeersch, and M. Z. Win, "Fundamental limits of wideband localization—Part II: Cooperative networks," *IEEE Trans. Inf. Theory*, vol. 56, no. 10, pp. 4981–5000, Mar. 2010.

[13] V. Navrátil, J. Krška, and F. Vejražka, "Concurrent bidirectional TDoA positioning in UWB network with free-running clocks," *IEEE Trans. Aerosp. Electron. Syst.*, vol. 58, no. 5, pp. 4434–4450, Oct. 2022.

[14] D. Feng, C. Wang, C. He, Y. Zhuang, and X.-G. Xia, "Kalman-Filter-Based integration of IMU and UWB for high-accuracy indoor positioning and navigation," *IEEE Internet Things J.*, vol. 7, no. 4, pp. 3133–3146, Apr. 2020.

[15] K. Wen, K. Yu, Y. Li, S. Zhang, and W. Zhang, "A new quaternion Kalman filter based foot-mounted IMU and UWB tightly-coupled method for indoor pedestrian navigation," *IEEE Trans. Veh. Technol.*, vol. 69, no. 4, pp. 4340–4352, Apr. 2020.

[16] M. Strohmeier, T. Walter, J. Rothe, and S. Montenegro, "Ultra-wideband based pose estimation for small unmanned aerial vehicles," *IEEE Access*, vol. 6, pp. 57526–57535, 2018.

[17] H. A. Hashim, L. J. Brown, and K. McIsaac, "Nonlinear stochastic attitude filters on the special orthogonal group 3: Ito and stratonovich," *IEEE Trans. Syst., Man, Cybern., Syst.*, vol. 49, no. 9, pp. 1853–1865, Sep. 2019.

[18] C. K. Chui and G. Chen, *Kalman Filtering*. Cham, Switzerland: Springer, 2017.

[19] M. Zamani, J. Trumpf, and R. Mahony, "Minimum-energy filtering for attitude estimation," *IEEE Trans. Autom. Control*, vol. 58, no. 11, pp. 2917–2921, Nov. 2013.

[20] J. L. Crassidis, F. L. Markley, and Y. Cheng, "Survey of nonlinear attitude estimation methods," *J. Guid., Control, Dyn.*, vol. 30, no. 1, pp. 12–28, Jan. 2007.

[21] H. A. Hashim, "Systematic convergence of nonlinear stochastic estimators on the special orthogonal group SO(3)," *Int. J. Robust Nonlinear Control*, vol. 30, no. 10, pp. 3848–3870, Jul. 2020.

[22] A. Barrau and S. Bonnabel, "The invariant extended Kalman filter as a stable observer," *IEEE Trans. Autom. Control*, vol. 62, no. 4, pp. 1797–1812, Apr. 2017.

[23] M. Hua and H. Liu, "Joint estimation of DOA and TOA for MB-OFDM UWB signals based on frequency-domain processing," *IET Radar, Sonar Navigat.*, vol. 10, no. 8, pp. 1337–1346, Oct. 2016.

[24] S. Bottigliero, D. Milanesio, M. Saccani, and R. Maggiora, "A low-cost indoor real-time locating system based on TDOA estimation of UWB pulse sequences," *IEEE Trans. Instrum. Meas.*, vol. 70, pp. 1–11, 2021.

[25] J. Sidorenko, V. Schatz, N. Scherer-Negenborn, M. Arens, and U. Hugentobler, "Error corrections for ultrawideband ranging," *IEEE Trans. Instrum. Meas.*, vol. 69, no. 11, pp. 9037–9047, Nov. 2020.

[26] F. L. Markley, "Attitude filtering on So(3)," *J. Astron. Sci.*, vol. 54, no. 3, pp. 391–413, 2006.

[27] S. Tong, Y. Li, Y. Li, and Y. Liu, "Observer-based adaptive fuzzy backstepping control for a class of stochastic nonlinear strict-feedback systems," *IEEE Trans. Syst., Man, Cybern., B, Cybern.*, vol. 41, no. 6, pp. 1693–1704, Dec. 2011.

[28] K. Ito and K. M. Rao, *Lectures on Stochastic Processes*. Mumbai, India: Tata institute of fundamental research, 1984, vol. 24.

[29] A. H. Jazwinski, *Stochastic Processes and Filtering Theory*. North Chelmsford, MA, USA: Courier Corp., 2007.

[30] H.-B. Ji and H.-S. Xi, "Adaptive output-feedback tracking of stochastic nonlinear systems," *IEEE Trans. Autom. Control*, vol. 51, no. 2, pp. 355–360, Feb. 2006.

[31] H. Deng, M. Krstic, and R. J. Williams, "Stabilization of stochastic nonlinear systems driven by noise of unknown covariance," *IEEE Trans. Autom. Control*, vol. 46, no. 8, pp. 1237–1253, Aug. 2001.

[32] C. Jiang, J. Shen, S. Chen, Y. Chen, D. Liu, and Y. Bo, "UWB NLOS/LOS classification using deep learning method," *IEEE Commun. Lett.*, vol. 24, no. 10, pp. 2226–2230, Oct. 2020.

[33] W. Zhao, A. Goudar, X. Qiao, and A. P. Schoellig, "UTIL: An ultra-wideband time-difference-of-arrival indoor localization dataset," *Int. J. Robot. Res.*, vol. 2022, pp. 1–11, Mar. 2022.

[34] T. Soderstrom, *Discrete-time Stochastic Systems: Estimation and Control*. Cham, Switzerland: Springer, 2002.

[35] P. S. Maybeck, *Stochastic Models, Estimation, and Control*. New York, NY, USA: Academic, 1982.

Hashim A. Hashim (Senior Member, IEEE) received the B.Sc. degree in mechatronics from the Department of Mechanical Engineering, Helwan University, Cairo, Egypt, the M.Sc. degree in systems and control engineering from the Department of Systems Engineering, King Fahd University of Petroleum and Minerals, Dhahran, Saudi Arabia, and the Ph.D. degree in robotics and control from the Department of Electrical and Computer Engineering, Western University, Ontario, Canada.

From 2019 to 2021, he was an Assistant Professor with the Department of Engineering and Applied Science, Thompson Rivers University, Kamloops, British Columbia, Canada. He is currently an Assistant Professor with the Department of Mechanical and Aerospace Engineering, Carleton University, Ottawa, Ontario. His current research interests include vision-based aided navigation and control, localization and mapping, stochastic and deterministic estimation, sensor fusion, and distributed control of multi-agent systems.

Abdelrahman E. E. Eltoukhy received the B.Sc. degree in production engineering from Helwan University, Egypt, the M.Sc. degree in engineering and management from Politecnico di Torino, Italy, and the Ph.D. degree from The Hong Kong Polytechnic University, Hong Kong.

Before joining The Hong Kong Polytechnic University, he was an Assistant Professor with the Systems Engineering Department, King Fahd University of Petroleum and Minerals, Dhahran, Saudi Arabia. Later, he moved to the Department of Industrial and Systems Engineering, The Hong Kong Polytechnic University, as a Research Assistant Professor. His current research interests include airline schedule planning, logistics and supply chain management, operations research, simulation, AI optimization, and robot localization and mapping.

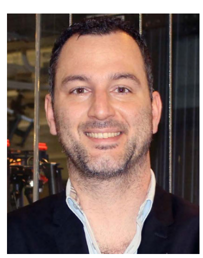

Kyriakos G. Vamvoudakis (Senior Member, IEEE) was born in Athens, Greece. He received the Diploma degree in electronic and computer engineering from the Technical University of Crete, Crete, Greece, in 2006, and the M.Sc. and Ph.D. degrees in electrical engineering from The University of Texas at Arlington, TX, USA, in 2008 and 2011, respectively.

From 2012 to 2016, he was a Research Scientist with the Center for Control, Dynamical Systems and Computation, University of California at Santa Barbara, Santa Barbara, CA, USA. He was an Assistant Professor with the Kevin T. Crofton Department of Aerospace and Ocean Engineering, Virginia Tech, Blacksburg, VA, USA, until 2018. He is currently an Assistant Professor with the Daniel Guggenheim School of Aerospace Engineering, Georgia Tech, Atlanta, GA, USA. His current research interests include reinforcement learning, game theory, cyber-physical security, and safe autonomy.

Dr. Vamvoudakis was a recipient of the 2019 ARO YIP Award, the 2018 NSF CAREER Award, the 2021 GT Chapter Sigma Xi Young Faculty Award, and several international awards, including the 2016 International Neural Network Society Young Investigator (INNS) Award.